Paper

A Microscopic Approach for THz Intersubband Challenges

Mauro F. Pereira

Abstract—The main candidate to be a practical and low cost high power THz source is the intersubband-based quantum cascade laser, which can have a tremendous impact in many practical applications, including last mile and indoor telecommunication systems. In this review we discuss current challenges for THz intersubband device development from a microscopic point of view. Next summarize the search for new mechanisms and structure designs that can lead to intersubband gain without population inversion. This is a very important topic of current research, since is both an extremely elegant phenomenon from the basic physics of view and crucial for effective lasing in the THz range. The reason is that scattering phenomena can lead to level broadenings of the same order of magnitude of the lasing transitions, making population inversion by carrier injection in upper lasing subbands extremely difficult. Previous work in the literature is compared and contrasted with a new scheme that may lead to high temperature lasing by engineering the nonequilibrium population inversion with a combination of band structure and many body effects mediated by a k-space filter.

Keywords—band structure engineering, coupled valence bands, intersubband laser, intersubband transitions, lasing without inversion, terahertz radiation.

1. Introduction

Intersubband optics and the terahertz (THz) range of the electromagnetic spectrum are the current frontiers in semiconductor science from both fundamental and applications points of view. To date the exploitation of THz waves has been largely underdeveloped due to the lack of a compact coherent source; providing high output power preferably with continuous wave (cw) operation. This is despite the huge potential THz technology has in a varied list of applications; detecting tumours and skin cancers, pharmaceutical applications, detecting and discriminating different explosive threat materials, environmental sensing and gas monitoring, industrial process control, as well as applications in astronomy, semiconductor imaging, security and medical imaging and telecommunication applications.

Due to the increasing demand for bandwidth it is expected that THz communication systems will be developed in a few years time. American and Japanese companies have already taken the first steps in this direction. Short-range indoor communication systems which work at carrier frequencies of a few hundred gigahertz will represent the wireless local area network (LAN) systems of the future. Such systems could also solve the current "last mile telecommunication" problem.

As a matter of fact, the demand for bandwidth in wireless short-range communication systems has doubled every 18 months over the last 25 years and there is no reason to expect that this trend would come to an end [1].

There are several different meanings for bandwidth and here it means the rate at which information can be transmitted over a given medium (telephone cables, cable TV, microwave relays, fiber optics, satellite links, etc.) In general the permissible bandwidth is about 0.1% to 1% of the carrier frequency. This means that the available bandwidth grows with the carrier frequency. In other words, the higher the frequency, the greater the volume of information that can be transmitted.

The current short-range communications systems Bluetooth and wireless LANs will not be able to deliver the bandwidth needed in 10 years because they operate with carrier frequencies of only a few gigahertz and the same happens for the currently emerging ultra wide band technology. Those systems are limited to rates below 1 Gbit/s. Future systems delivering data rates above 10 Gbit/s will have to work at several ten or preferably a few hundred GHz and this will require higher carrier frequencies. The use of bandwidth is regulated in the USA up to frequencies of 300 GHz with a window from 275 to 300 GHz which is reserved for communications [2]. In Europe the allocation is the same but ends at 275 GHz. In other words, there is free communication bandwidth available above 275 GHz. Systems operating at those frequencies are already in the THz range. Thus, compact and inexpensive devices emitting in this range are required. The quantum cascade laser (QCL) is a potential candidate.

The first mid infra red (MIR) QCL was demonstrated in 1994 by Faist *et al.* at Bell Labs [3] and the extension of the QCL design to emission frequencies below the Restrahlen band was achieved in 2002 when Köhler *et al.* [4] demonstrated the first THz QCL, at 4.4 THz. Since then they have achieved a maximum operating temperature of 186 K [5].

Even though intersubband emitters are the best candidate as compact high power sources for THz radiation, a current review of the field seems to indicate that conventional designs for QCLs emitting at a given energy $\hbar\omega$ appear to have an maximum operating temperature $T_{\max} \approx \hbar\omega/k_B$ [6]. Thus attainment of room temperature operation seems unlikely without external cooling. Dramatic progress can only be achieved with deep understanding and unconventional manipulation of microscopic mechanisms.

Figure 1 illustrates some of the microscopic difficulties that prevent current THz QCLs to operate at room temperature at high output power. The most critical issue currently

limiting THz QCLs as widely exploitable imaging sources is achieving population inversion at high temperatures depicted in Fig. 1(a)–(d).

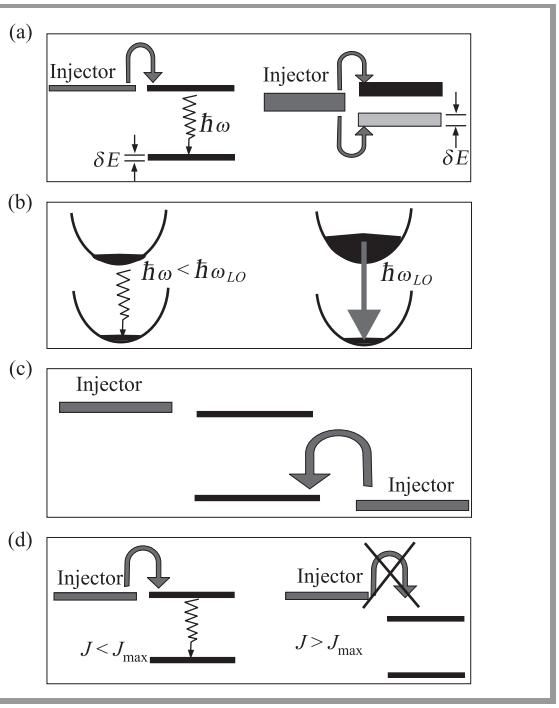

Fig. 1. Cartoon of the most critical issue currently limiting THz QCLs as widely exploitable imaging sources is achieving population inversion at high temperatures.

In Fig. 1(a), in contrast to the mid-IR case (left diagram), for THz transitions (right diagram) the energy difference between the lasing levels is not much larger than the level broadening. The electrons can tunnel from the injector to the upper or lower levels reducing population inversion. In Fig. 1(b), in the right-hand diagram the temperature is high. The upper subband is occupied up to electronic states with sufficient energy to emit longitudinal-optic (LO) phonons, and thus decay nonradiatively to the lower lasing level, reducing the population inversion. In Fig. 1(c), thermal backfilling of the lower radiative state by carriers from the injector states reduces population inversion at high temperatures. In Fig. 1(d), at high temperatures beyond the peak bias level when the maximum achievable current $J_{\max}$ is reached, the injector and upper levels get misaligned and the device ceases to operate.

2. Lasing Without Population Inversion

Lasing without inversion (LWI) is a new solution for producing laser light and it has been achieved in gas and semiconductor lasers, opening new possibilities for cleverly sidestepping traditional difficulties of producing radiation in both extremes of the spectrum: ultraviolet and x-ray lasing on the high energy side and far infrared (TERA-MIR) in the low energy range. In a gas of atoms, laser light buildup begins when a single photon, emitted by an atom in a high-energy (excited) state, stimulates other excited atoms to emit photons with identical attributes. Ordinary lasers normally require the energy-intensive process of "population inversion", in which a majority of the atoms must be excited into a high-energy state. Promoting atoms into excited states prepares them for participating in the laser process, but it also serves to prevent them from soaking up the light and thereby sabotaging the laser process.

However, maintaining a population inversion in ultraviolet and x-ray lasers is extremely difficult because the high-lying excited states necessary to produce such light are so short-lived. To the best of the author's knowledge, the first demonstration of lasing without inversion appeared in atomic optics and was based on quantum interference in Rb atoms [7]. Previous experiments had produced nanosecond bursts of light without population inversion, but the paper [7] was the first to report a sustained laser beam through LWI. In these experiments, an external laser beam essentially creates two pathways for the atoms to get from the ground state ($|a\rangle$) to the excited state ($|b\rangle$). In the rubidium experiment, for example, the probability of getting atoms from ($|a\rangle$) to ($|b\rangle$) becomes the overlap of the likelihood of getting from state ($|a\rangle$) to state ($|b\rangle$) directly and going from state a to an even higher excited state ($|c\rangle$) then decaying to state ($|b\rangle$). Under the proper conditions, the overlapping likelihoods can interfere so as to cancel each other out, preventing absorption. In other words, effective LWI in atomic systems has been based on quantum interference. Future goals are to achieve LWI in inexpensive diode lasers (like those in CD players) and to produce x-ray and UV light through LWI. Here we analyse a very different scenario in intersubband emitters [8]–[10]. This may turn out crucial in the search for room temperature THz QCLs. The main reason for this is that dephasing and scattering phenomena can lead to level broadenings of the same order of magnitude of the lasing transitions, making population inversion by carrier injection in upper lasing subbands extremely difficult, as depicted in the cartoons of Fig. 1.

The first experimental realization of intersubband lasers without inversion exploited the nonparabolicity of the conduction subbands and local population inversion near $k = 0$ even though the lowest subband may have larger global occupation [10].

Later on, valence-band-based designs have been proposed [11]–[13]. Intervalence band emitters based on Si-Ge structures have been investigated. However, lasing on quantum cascade structures has never been demonstrated. Only electroluminescence has been measured so far [14]–[16]. A complete set parameters required for predictive calculations of optical properties of Si-Ge devices is still not known, although progress in this direction has been recently achieved [17]. On the other hand, the material parameters for the III-V system investigated here are very well known. This review complements the results given recently in [18], [19] comparing and contrasting the results for two different well widths.

The following features are unique of the approach introduced in [18] and were not found in previous studies in the literature:

- The strongly k-dependent transverse-electric (TE) transition is used to create a k-space filtering effect that enhances the gain due to local population inversion that arises due to the strongly nonparabolicity of the valence bands.
- The nonequilibrium Keldysh Green's function method is used allowing the consideration of dephasing effects.
- Detrimental cross-absorption due to multiple transitions is taken into account.

Another useful feature of the approach is that simple surface emitting designs can be constructed due to the TE polarization of the emitted field.

3. Numerical Results and Discussion

Necessary conditions to obtain lasing without inversion exploiting nonparabolicity are that the upper conduction subband should either have smaller effective mass or cooler electrons. For unstrained GaAs-AlGaAs wells, even though the conduction bands can be characterized by effective masses (parabolic) "nonparabolicity" appears with different effective masses per subband. And usually the lowest band has a lighter effective mass. The valence bands in contrast have typically lower averaged effective masses in the upper lasing subband which is an advantage. However, as the nonparabolicity can be in some cases so strong that an effective mass does not make sense and the full dispersions must be used, which can complicate the numerical calculations enormously, specially if many particle and dephasing effects are taken into account [18], [19].

The model system investigated in this paper is globally out of equilibrium but the holes are assumed to be thermalized within each subband with occupation functions characterized by different temperatures. The temperatures of the electrons (or holes) in different subbands can be different. This fact has as determined experimentally for conduction band designs by means of microprobe photoluminescence experiments [20]. It is a design challenge to cool the upper subband electrons for more efficient lasing. Furthermore the number of carriers in each subband in an intersubband system depends on the injection scheme and can be chosen independently of the temperature in simulations, see, e.g., [18].

The results shown next are all for non-global inversion conditions and $GaAs/Al_{0.3}Ga_{0.7}As$ quantum wells. Only the top two valence subbands 1 and 2 are occupied and in all cases the lowest hole band has equal or more total carrier density than the upper (lasing) hole subband, i.e., $n_2 \leq n_1$. Detrimental cross absorption due to higher (empty) hole subbands is taken into account. Before proceeding further the following point should be highlighted: very good agreement with experiments has been obtained by considering electron-phonon and electron-impurity scattering as the main origin of dephasing in mid infrared systems [21]–[23]. Interface roughness scattering also plays a role even in THz systems, however, this effect depends on sample quality [24], [25] and the inclusion of sample quality considerations would be beyond the scope of this paper.

The nature of the main non-radiative channel between subbands, which is crucial to the device performance, remains a matter of controversy for THz systems. The typical energy spacing for one active region period is lower than the optical phonon energy (36 meV in GaAs). Thus, optical phonon emission may not always be the dominant non-radiative mechanism unless the electrons are very hot. Moreover, many-body effects (electron-electron scattering resonances) have been observed in recent experiments for THz QCLs operating in the quantum Hall regime [26]. Thus in the theoretical limit analyzed in this paper, the dephasing is due only to electron-electron mechanisms [27]. Consideration of other scattering channels will be the subject of future research.

The optical properties in which we are interested are calculated in our approach through the optical susceptibility, χ, which can be directly obtained from the Green's function G. The absorption $\alpha(\omega)$ and gain spectra $g(\omega) = -\alpha(\omega)$ are calculated from the imaginary part of the optical susceptibility $\chi(\omega)$ (see, [18]):

$$\begin{aligned} \alpha(\omega) &= \frac{4\pi\omega}{cn_b}\Im\{\chi(\omega)\}, \\ \chi(\omega) &= 2\sum_{\mu\neq\nu,\vec{k}} \wp_{\mu\nu}(k)\,\chi_{\nu,\mu}(k,\omega). \end{aligned} \tag{1}$$

Here n_b denotes the background refractive index, c is the speed of light, $\wp_{\nu\mu}(k) = ed_{\nu\mu}(k)$ is the transition dipole moment between the subbands ν and μ, which are labelled $\mu = 1,2,\ldots$ from the top valence band. Thus in the discussion that follows, if holes are injected in the subband 2 and make a transition to subband 1 creating a photon, this actually means that an electron made a transition from valence subband 1 to subband 2 and will be called a (2,1) transition.

The nonequilibrium steady-state susceptibility function $\chi_{\nu\mu}(k,\omega)$ is evaluated through the carriers Keldysh Green's function G, whose time evolution is described by a Dyson equation. The resulting integro-differential equation for $\chi_{\nu\mu}(k,\omega)$ is solved numerically in this paper including many body effects at the Hartree-Fock level, complex nonparabolic band structure, correlation and dephasing mechanisms.

The numerical scheme used here can be summarized as follows: the first step is the solution of the 8×8 $\mathbf{k}\cdot\mathbf{p}$ Hamiltonian [27]. The Green's functions and self-energies are expanded using eigenstates and eigenvalues of this Hamiltonian. Next, by assuming thermalized holes, the full nonequilibrium Green's function (NEGF) scheme is simplified and reduces to the self-consistent evaluation of chemical potentials and self-energy matrix elements which lead

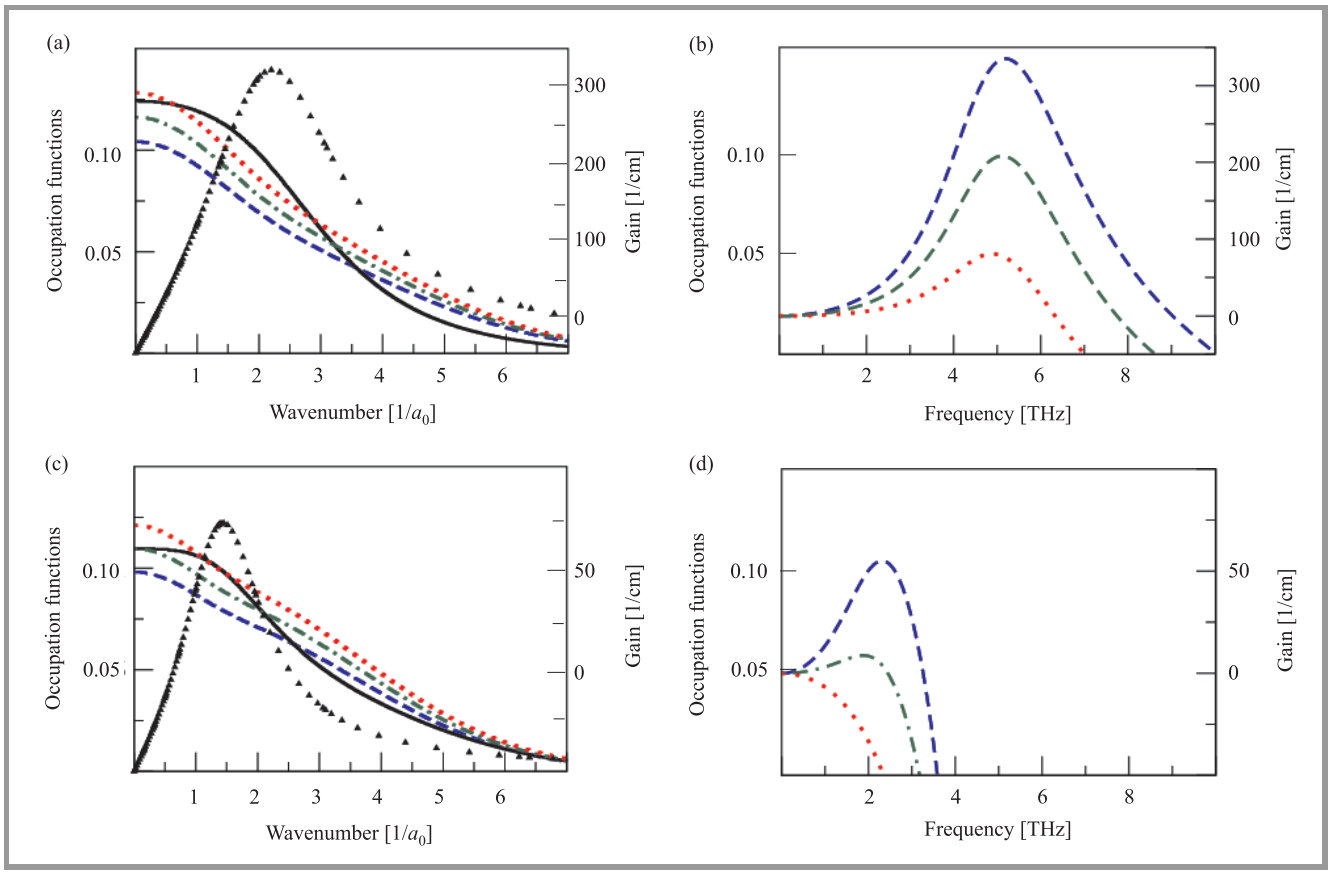

Fig. 2. Comparison of occupation functions and transition dipole moments (symbols) in (a), (c) against gain spectra in (b), (d). The two quantum wells considered have widths of 5 nm (a), (b) and 10 nm (c), (d). The wavenumber is presented in units of $1/a_0$, where a_0 is the 2D Bohr radius.

to subband energy renormalizations, dephasing constants and occupation functions. Only carrier-carrier scattering is considered here and details of the corresponding self-energy are given in [27].

Finally, absorption and gain are given by the solution of the integro-differential equation obtained from the carriers Green's function by numerical matrix inversion. The susceptibility function can be written as

$$\chi_{v\mu}(k,\omega) = \sum_{\mathbf{k}'\neq\mathbf{k}} \left(M_{kk'}^{v\mu}\right)^{-1} \wp_{v\mu}(k')\delta n_{v\mu k'}, \qquad (2)$$

where $\left(M_{k'k}^{v\mu}\right)^{-1}$ is the inverse of

$$\begin{aligned} M_{kk'}^{v\mu} \;=\; & \left(\hbar\omega - e_{v\mu}(k) + i\Gamma_{v\mu}\right)\delta_{k,k'} \\ & + \left(1-\delta_{k,k'}\right)\delta n_{v\mu k}\tilde{V}_{\mathbf{k}-\mathbf{k}'}^{v\mu}. \end{aligned} \qquad (3)$$

Here $\delta n_{v\mu k} = n_v(k) - n_\mu(k)$ denotes the nonequilibrium population difference between subbands v and μ. Further details of the renormalized energies $e_{v\mu}$, electron-electron scattering broadening $\Gamma_{v\mu}$ and the Coulomb matrix elements $\tilde{V}_{\mathbf{k}-\mathbf{k}'}^{v\mu}$ are given in [21], [27]. The role of the dipole function $\wp_{v\mu}(k')$ as a k-space filter is then clear in Eq. (2). The overlap of a strongly peaked dipole function exactly where local population inversion $\delta n_{v\mu k'}$ takes place enhances the gain without inversion effect as illustrated by Fig. 2. More details of the numerical method are given in [18].

Figure 2 compares and contrasts the occupation functions and gain spectra for two different quantum wells. An important remark should be made before analyzing the numerical results. The gain spectra are inversely proportional to the period length. The period used here is the quantum well width, $L_c = 5$ nm or 10 nm consistently with the model. In actual QCLs, the period is extended to include barriers, injector, and collectors, and it can easily be at least 5 as large. Since the number of photons emitted per period remains constant this means that the gain spectra calculated here are very high in comparison to what should be expected in actual QCL structures. Note, however, that the qualitative analysis that follows is fully consistent with the single quantum well model.

The occupation functions are given on the left and corresponding gain spectra on the right panels for 5 nm (top) and 10 nm (bottom) GaAs-$Al_{0.3}Ga_{0.7}As$ quantum wells. Only the two top subbands are occupied and in both subbands the electrons are thermalized at $T = 300$ K. In both panels in the left the triangle symbols are the corresponding transition dipole moments for the (1,2) transition respon-

sible for the gain. The dipoles have been scaled in the y-axis to fit in the plot. The solid curve is the occupation of the upper subband, fixed in all gain calculations at $n_2 = 4 \cdot 10^{11}$ carriers/cm^2. From bottom to top, the dashed, dot-dashed and dotted curves are for increasing lower hole subband total occupation density $n_1 = 4$, 4.5 and $5 \cdot 10^{11}$ carriers/cm^2.

The corresponding gain curves are easily identified on the right and correspond to the densities in the second subband. In other words, from top to bottom, the dashed, dot-dashed and dotted curves are for increasing lower hole subband total occupation density $n_1 = 4$, 4.5 and $5 \cdot 10^{11}$ carriers/cm^2. The gain decreases as the lower occupation increases. The transition dipole moment, which has a strong filtering effect in k-space is scaled to fit in the plots. Following intuition, the gain decreases as the global occupation of the lower band increases. The 5 nm quantum well leads to better local inversion assuming that the same 2D density can be achieved in both samples and leads to more robust gain against increases in the lower subband carrier density.

However, in an actual structure it may be more difficult to inject the same global density of electrons for 5 nm then for 10 nm. More realistic calculations will be performed with a new generation of our NEGFs simulator, which will be capable of describing valence band cascaded structures and will be the subject of future publications.

In summary, this manuscript reviewed a possible solution for intersubband emitters that can lead to revolutionary devices for the completely open field of THz telecommunications and many other applications.

References

[1] S. Cherry, "Edholm's law of bandwidth", *IEEE Spectr.*, vol. 41, pp. 58–59, 2004.

[2] M. Koch, "IN-door THz communications: a vision for 2020", in *Terahertz Frequency Detection and Identification of Materials and Objects*, R. E. Miles *et al.*, Eds. Nato Security Through Science Series. Berlin: Springer, 2007, pp. 325–338.

[3] J. Faist, F. Capasso, D. L. Sivco, C. Sirtori, A. L. Hutchinson, and A. Y. Cho, "Quantum cascade laser", *Science*, vol. 264, no. 5158, pp. 553–556, 1994.

[4] R. Köhler, A. Tredicucci, F. Beltran, H. E. Beere, E. H. Linfield, A. Davies, D. A. Ritchie, R. Iotti, and F. Rossi, "Terahertz semiconductor-heterostructure laser", *Nature*, vol. 417, no. 6885, pp. 156–159, 2002.

[5] S. Kumar, Q. Hu, and J. Reno, "186 K operation of terahertz quantum-cascade lasers based on a diagonal design", *Appl. Phys. Lett.*, vol. 94, no. 13, pp. 131105-1–1331105-3, 2009.

[6] B. S. Williams, "Terahertz quantum-cascade lasers", *Nat. Phot.*, vol. 1, no. 9, pp. 517–525, 2007.

[7] A. S. Zibrov, M. D. Lukin, D. E. Nikonov, L. Hollberg, M. O. Scully, V. L. Velichansky, and H. G. Robinson, "Experimental demonstration of laser oscillation without population-inversion via quantum interference and in RB", *Phys. Rev. Lett.*, vol. 75, no. 8, pp. 1499–1502, 1995.

[8] A. Wacker, "Coexistence of gain and absorption", *Nat. Phys.*, vol. 3, no. 5, pp. 298–299, 2007.

[9] R. Terazzi, T. Gresch, M. Giovanni, N. Hoyler, F. Faist, and N. Sekine, "Bloch gain in quantum cascade laser", *Nat. Phys.*, vol. 3, no. 5, pp. 329–333, 2007.

[10] J. Faist, F. Capasso, C. Sirtori, D. L. Sivco, A. L. Hutchinson, M. S. Hybertsen, and A. Y. Cho, "Quantum cascade lasers without intersubband population inversion", *Phys. Rev. Lett.*, vol. 76, no. 3, pp. 411–415, 1996.

[11] G. Sun, A. Liu, and J. B. Khurgin, "Valence intersubband lasers with inverted light-hole effective mass", *Appl. Phys. Lett.*, vol. 72, no. 12, pp. 1481–1483, 1998.

[12] L. Friedman, G. Sun, and A. Soref, "SiGe/Si THz laser based on transitions between inverted mass light-hole and heavy-hole subbands", *Appl. Phys. Lett.*, vol. 78, no. 4, pp. 401–403, 2001.

[13] R. A. Soref and G. Sun, "Terahertz gain in a SiGe/Si quantum staircase utilizing the heavy-hole inverted effective mass", *Appl. Phys. Lett.*, vol. 79, no. 22, pp. 3639–3641, 2001.

[14] G. Dehlinger, L. Diehl, U. Gennser, H. Sigg, J. Faist, K. Ensslin, D. Grutzmacher, and E. Muller, "Intersubband electroluminescence from silicon-based quantum cascade structures", *Science*, vol. 290, no. 5500, p. 2277, 2000.

[15] L. Diehl, S. Mentese, E. Müller, D. Grützmacher, H. Sigg, U. Gennser, I. Sagnes, Y. Campidelli, O. Kermarrec, D. Bensahel, and J. Faist, "Electroluminescence from strain-compensated $Si_{0.2}Ge_{0.8}$/Si quantum-cascade structures based on a bound-to-continuum transition", *Appl. Phys. Lett.*, vol. 81, no. 25, pp. 4700–4702, 2002.

[16] R. Bates, S. A. Lynch, D. Paul, Z. Ikonic, R. W. Kelsall, P. Harrison, S. L. Liew, D. J. Norris, A. G. Cullis, W. R. Tribe, and D. D. Arnone, "Interwell intersubband electroluminescence from Si/SiGe quantum cascade emitters", *Appl. Phys. Lett.*, vol. 83, no. 20, pp. 4092–4094, 2003.

[17] D. J. Paul, "8-band k · p modeling of the quantum confined Stark effect in Ge quantum wells on Si substrates", *Phys. Rev. B*, vol. 77, no. 15, pp. 155323-1–155323-7, 2008.

[18] M. F. Pereira Jr., "Intervalence transverse-electric mode terahertz lasing without population inversion", *Phys. Rev. B*, vol. 78, no. 24, pp. 245305-1–245305-5, 2008.

[19] M. F. Pereira, "Valence intersubband gain without population inversion", *Centr. Eur. J. Phys.*, DOI: 10.2478/s11534-009-0061-5 (in press) [Online]. Available: http://www.springerlink.com/content/j9nm0k6179g142n6/

[20] M. S. Vitiello, G. Scamarcio, V. Spagnolo, B. S. Williams, S. Kumar, Q. Hu, and J. L. Reno, "Measurement of subband electronic temperatures and population inversion in THz quantum-cascade lasers", *Appl. Phys. Lett.*, vol. 86, no. 111115–111117, 2005.

[21] M. F. Pereira Jr., S.-C. Lee, and A. Wacker, "Controlling many-body effects in the midinfrared gain and terahertz absorption of quantum cascade laser structures", *Phys. Rev. B*, vol. 69, p. 205310, 2004.

[22] R. Nelander, A. Wacker, M. F. Pereira Jr., D. G. Revin, M. R. Soulby, L. R. Wilson, J. W. Cockburn, A. B. Krysa, J. S. Roberts, and R. J. Airey, "Fingerprints of spatial charge transfer in quantum cascade lasers", *J. Appl. Phys.*, vol. 102, no. 11, pp. 113104-1–113104-5, 2007.

[23] M. F. Pereira Jr, R. Nelander, A. Wacker, D. G. Revin, M. R. Soulby, L. R. Wilson, J. W. Cockburn, A. B. Krysa, J. S. Roberts, and R. J. Airey, "Characterization of intersubband devices combining a nonequilibrium many body theory with transmission spectroscopy experiments", *J. Mater. Sci. Mater. Electron.*, vol. 18, no. 7, pp. 689–694, 2007.

[24] A. Wacker, "Coherence and spatial resolution of transport in quantum cascade lasers", *Phys. Stat. Sol. C*, vol. 5, no. 1, pp. 215–220, 2008.

[25] T. Kubis, "Quantum theory of transport and optical gain in quantum cascade lasers", *Phys. Stat. Sol. C*, vol. 5, no. 1, pp. 232–235, 2008.

[26] G. Scalari, S. Blaser, J. Faist, H. Beere, E. Linfield, D. Ritchie, and G. Davies, "Terahertz emission from quantum cascade lasers in the quantum Hall regime: evidence for many body resonances and localization effects", *Phys. Rev. Lett.*, vol. 93, no. 23, pp. 237403-1–237403-4, 2004.

[27] M. F. Pereira Jr. and H. Wenzel, "Interplay of Coulomb and nonparabolicity effects in the intersubband absorption of electrons and holes in quantum wells", *Phys. Rev. B*, vol. 70, no. 20, pp. 205331-1–205331-8, 2004.

Mauro F. Pereira was born in Rio de Janeiro, Brazil. He received the B.Sc. in physics at PUC/RJ (1983) and the M.Sc. in physics (1985). He completed the Ph.D. in optical sciences at the Optical Sciences Center in Tucson/AZ in 1992 and received an equivalent Dr. Sci. degree in physics from UFRJ in 1993. He was a Research Associate at PUC/RJ, CBPF, Uni-Rostock, and the TU-Berlin, an invited lecturer in Bremen, an Associate Professor at UFBA and a Senior Researcher at Tyndall National Institute before joining the Materials and Electrical Engineering Research Institute of Sheffield Hallam University as a Professor. His expertise includes nonlinear and quantum optics, exciton and polariton effects, band structure engineering, many-body effects, semiconductor lasers including quantum cascade structures, nonequilibrium Green's functions, quantum transport and numerical methods. The results are aimed at fundamental understanding and as input for the design and simulation of novel optical and electrooptical devices.

e-mail: M.Pereira@shu.ac.uk
Materials and Engineering Research Institute
Sheffiled Hallam University
S1 1WB, Sheffield, United Kingdom